Angular modulation of nonlinear Breit-Wheeler yield by vacuum dichroism

Jia-Ding Chen,[1] Ya-Nan Dai,[2] Kai-Hong Zhuang,[1] Jing-Jing Jiang,[1] Baifei Shen,[1] and Yue-Yue Chen[1,*]

[1]*Department of Physics, Shanghai Normal University, Shanghai 200234, China*

[2]*Shenzhen Key Laboratory of Ultraintense Laser and Advanced Material Technology, Center for Intense Laser Application Technology, and College of Engineering Physics, Shenzhen Technology University, Shenzhen 518118, China*

(Received 6 September 2024; accepted 24 December 2024; published 21 February 2025)

Vacuum polarization is numerically investigated for the interaction between a GeV electron beam and a counterpropagating ultraintense laser pulse in the quantum radiation-dominated regime. We identify a signal of vacuum polarization in pair density using a straightforward one-stage setup, circumventing the challenge of preparations of highly polarized probe photons or precise measurements of photon polarization. In our scheme, most electrons are scattered in the direction of laser propagation while emitting substantial linearly polarized gamma photons. These photons undergo vacuum birefringence and dichroism before decaying into electron-positron pairs via the nonlinear Breit-Wheeler process. We demonstrate that vacuum dichroism enhances the purity of linear polarization, which suppresses the overall yield of electron-positron pairs and allows energetic photons to penetrate deeper into the laser pulse. The pairs produced by these energetic photons are more likely to be deflected into small-angle regions rather than being reflected, leading to an enhancement of pair yield in forward scattering. The difference in positron yield may have potential applications in measuring vacuum polarization effect in future laser-particle experiments.

DOI: 10.1103/PhysRevD.111.036025

Vacuum birefringence, a long-predicted effect in quantum electrodynamics (QED), remains unobserved in terrestrial experiments utilizing real photons [1–4]. Several ongoing experiments aim to detect the ellipticity signal of vacuum birefringence using optical photons and long magnetic field [1–6]. Noteworthy examples include the PVLAS [1,4] and BMV [3] experiments, which, despite significant progress, have yet to overcome challenges related to background noise [2,3]. An alternative strategy involves using high-powered laser facilities to polarize the vacuum, with an x-ray free-electron laser serving as the probe (see, for instance, the planned Helmholtz International Beamline for Extreme Fields [7] and station of extreme light [8,9] experiments).

The nonlinearity of the QED vacuum becomes significantly more pronounced for high-energy photons and intense external field, sparking interest in detecting vacuum polarization (VP) with a combination of high-power laser facilities and gamma probe photons [10–13]. The use of a gamma-ray probe brings the interaction into the high-energy nonperturbative regime, where the Euler-Heisenberg effective Lagrangian method becomes invalid for describing vacuum birefringence [12]. In this case, the QED photon polarization operator in the presence of a strong background field must be employed [12,14–19]. With the one-loop QED probability, a simulation method applicable to investigating high-energy vacuum polarization has been developed recently [20]. In the high-energy regime, the vacuum exhibits both birefringence and dichroism. The vacuum dichroism corresponds to the imaginary part of polarization operator, which is related to the pair production probability via the optical theorem, and the vacuum birefringence corresponds to the real part of the polarization operator. The imaginary part and real part are related via Kramers-Kronig relations [21,22]. Therefore, the relationship between tree-level and loop processes implies that observing pair yield corresponds to detecting nonlinear vacuum birefringence [23,24].

Detecting VP with a gamma probe typically involves a two-stage setup: First, polarized gamma probes are generated via linear Compton scattering of a week laser [10,12,20] or bremsstrahlung in a diamond crystal radiator target [24,25]; then, the highly polarized gamma photons are selected by angle to collide with a high-power laser. A change in photon polarization serves as evidence of VP. However, the first stage may introduce experimental errors and additional complexity to the experimental setup [26]. Additionally, such experiments require gamma-ray polarimetry and face a challenge in separating photonic signal

*Contact author: yue-yue.chen@shnu.edu.cn

from background, such as laser photons and secondary emissions of produced pairs.

To circumvent these challenges posed by photonic signals, one solution is to measure the polarized nonlinear Breit-Wheeler process [20,23,24]. The vacuum birefringence affects the polarization of probe gamma photons and, consequently, impacts the spin polarization of produced pairs. The positrons (electrons) are easier to measure than photons within a photon background, and the experimental detection capacity for leptons spin polarization (typically, ∼0.5% [27]) is currently much higher than that for γ polarization (typically, $\lesssim$10% [28]). A measurement of pair polarization [20] or the pair yield for different polarization states [24] may open a new way of testing vacuum birefringence. Unfortunately, these proposals still rely on the two-stage setup and polarization measurements. The high-energy photons generated in the first stage must be separated from the scattered electrons using a 1-m-long dipole magnet before being directed to a strong-field interaction point (IP) located several meters downstream of the radiator. The angular spectrum of the generated photons follows $1/\gamma$, which corresponds to ∼30 μrad for $\gamma = 16.5\ \mathrm{GeV}/m_e$. Consequently, the beam size at the IP is around 230 μm, significantly larger than the typical beam size of strong laser ($w_0 = 5$–25 μm) [26]. Therefore, only 0.3% of the prepared photons fall within ±25 μm at the IP, and this fraction decreases quadratically with decreasing laser spot size. Consequently, the pair production yield is quite low due to this spatial mismatch, which hinders accurate measurement of vacuum polarization. More importantly, the experimental feasibility of previous schemes remains restricted by the capacity for polarization measurement, highlighting the significant interest in identifying more viable physical observables. Recently, the STAR Collaboration has reported that angular modulation of the *linear* Breit-Wheeler pair creation yield in ultraperipheral heavy-ion collision experiments could be attributed to vacuum birefringence, implying a possible detection of vacuum nonlinearity using unpolarized measurement [23].

In this paper, we numerically investigate the collision between an ultrarelativistic unpolarized electron beam and a linearly polarized laser pulse. The electrons emit high-energy gamma photons via nonlinear Compton scattering, which subsequently annihilate into electron-positron pairs through the nonlinear Breit-Wheeler process. Vacuum dichroism enhances the linear polarization of intermediate photons, resulting in a reduced pair production rate. In a reflection scenario, the angular distribution of the produced pairs is influenced by VP: The overall positron density decreases, while the density concentrated in the small-angle region increases. Contrary to conventional approaches, where VP effects (VPEs) are observed through changes in the polarization of photons or produced pairs, we examine the impact of QED vacuum nonlinearity on pair yield without requiring polarization measurement.

The high-energy VPE is explored through a recently developed Monte Carlo simulation method that incorporates both vacuum birefringence and vacuum dichroism [20]. At each time step, the pair production is determined by the photon polarization-resolved pair production probability using the common algorithms [20,29–36]. If pair production is rejected, the photon's polarization state changes due to vacuum birefringence and vacuum dichroism. The vacuum birefringence is implemented via a polarization rotation between Stokes parameters ξ_1 and ξ_2 [12,20]:

$$\begin{pmatrix} \xi_1^f \\ \xi_2^f \end{pmatrix} = \begin{pmatrix} \cos\varphi & \sin\varphi \\ -\sin\varphi & \cos\varphi \end{pmatrix} \begin{pmatrix} \xi_1 \\ \xi_2 \end{pmatrix}, \tag{1}$$

where $\varphi = \frac{\alpha m^2}{\omega^2}\Delta t \int d\varepsilon \frac{\mathrm{Gi}'(\rho)}{\rho}$, with $\mathrm{Gi}'(x)$ being the derivative of the Scorer function, $\rho = [\delta(1-\delta)\chi_\gamma]^{-2/3}$, $\delta = \varepsilon/\omega$, and $\chi_\gamma = |F_{\mu\nu}k^\nu|/mF_{cr}$ being the strong-field quantum parameter. Here, ω and ε represent the energies of the photon and the produced electron, respectively. In this way, vacuum birefringence is incorporated at each time step rather than being derived from the final yield of pairs via Hilbert transformation [24]. This approach is, therefore, more suitable for a time-dependent analysis of loop effects and investigating vacuum polarization when high-order processes (e.g., pair creation by secondary photons) could influence the final yield of pairs.

Meanwhile, photons with different polarization states are absorbed at varying rates due to the photon polarization-dependent pair production probability. This selective effect on the initial photon polarization can cause polarization changes in the surviving particles, a phenomenon known as vacuum dichroism. In our simulation, vacuum dichroism is modeled by updating photon polarization $\boldsymbol{\xi}$ to ξ_f^{NP} at each time step. ξ_f^{NP} represents the photon polarization state determined by the no-pair production probability [20]:

$$\begin{aligned} \xi_f^{NP} &= \frac{\boldsymbol{\xi}(1-\underline{w}\Delta t) - \underline{\boldsymbol{f}}\Delta t}{1-\{\underline{w}+\underline{\boldsymbol{f}}\cdot\boldsymbol{\xi}\}\Delta t}, \\ \underline{w} &= \int \frac{\alpha m^2 d\varepsilon}{\sqrt{3}\pi\omega^2}\left[\int_{z_p}^{\infty} dx \mathrm{K}_{\frac{1}{3}}(x) + \frac{\varepsilon_+^2+\varepsilon^2}{\varepsilon\varepsilon_+}\mathrm{K}_{\frac{2}{3}}(z_p)\right], \\ \underline{\boldsymbol{f}} &= -\int \frac{\alpha m^2 d\varepsilon}{\sqrt{3}\pi\omega^2}\hat{e}_3 \mathrm{K}_{\frac{2}{3}}(z_p), \end{aligned} \tag{2}$$

where $z_p = \frac{2}{3\chi_\gamma}\frac{\omega^2}{\varepsilon_+\varepsilon}$ with ε_+ being positron energy and $\hat{e}_3 = (0,0,1)$. It has been demonstrated that the no-pair production probability is equivalent to the α-order loop probability related to vacuum dichroism [18,20]. This algorithm for incorporating radiative corrections to photon self-energy aligns with the one used for electron self-energy [37,38].

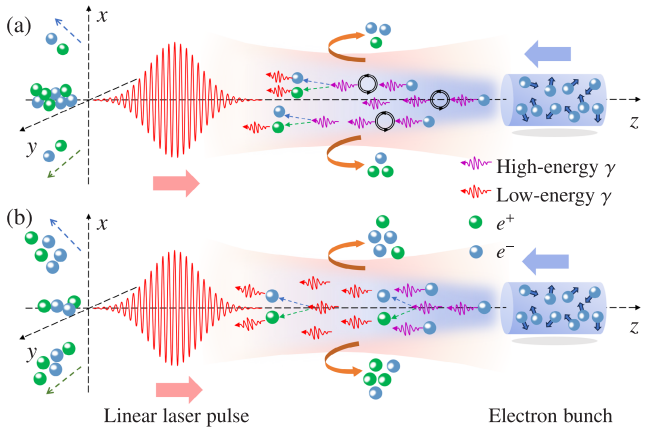

FIG. 1. (a) Scheme for measuring vacuum polarization effect. The linearly polarized laser pulse head-on collision with an unpolarized GeV electron beam. The nonlinear Compton scattering and nonlinear Breit-Wheeler take place within the volume where the pulse and the bunch overlap. During the interaction, most pairs are reflected in the $+z$ direction, while some continue to propagate forward. (b) The same as (a) but with the vacuum polarization effect artificially turned off. Without vacuum polarization, the yield of pairs in the small-angle region decreases.

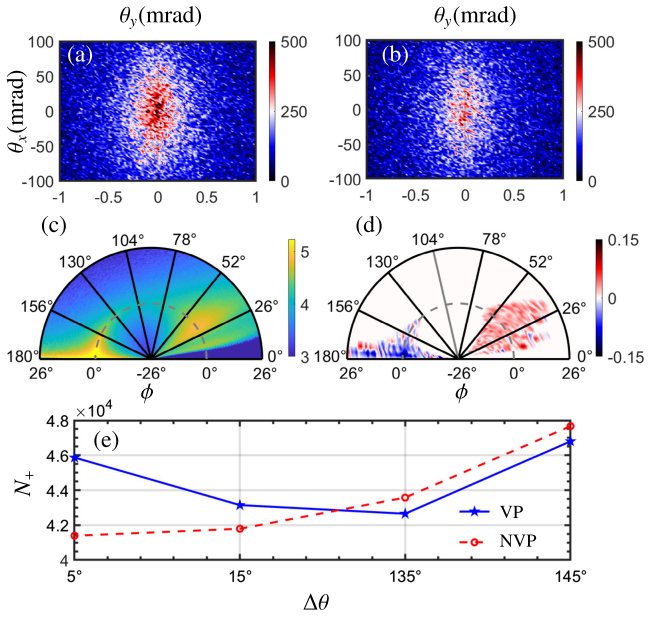

FIG. 2. The angular distribution of positron density $d^2N_+/d\theta_x d\theta_y$ within $|\theta_x| \lesssim 100$ mrad and $|\theta_y| \lesssim 1$ mrad versus $\theta_x = \tan^{-1} p_x/p_z$ (mrad) and $\theta_y = \tan^{-1} p_y/p_z$ (mrad) for the cases with (a) and without (b) VPE. Angular distribution of positrons density $\log_{10}(dN_+/d\Omega)$ (c) and density difference R (d) versus the polar angle θ (degree, black solid scale) and azimuthal angle ϕ (degree, gray dashed scale). (e) The scaling law of positron yield N_+ within $\delta\theta = 10°$ and $\phi \in (-1°, 1°)$ versus deflection angle $\Delta\theta = \pi - \theta$ for the cases with (blue solid line) and without (red dashed line) VPE.

Under the local-constant field approximation, the polarization operator is nonzero only when the external photon four-momentum is conserved [17]. Consequently, off-forward scattering does not occur in strong-field conditions, and the photon's momentum and energy remain unchanged at each time step.

We consider an ultrarelativistic electron beam with energy $\varepsilon_0 = 10$ GeV colliding with a focused linearly polarized strong laser field with intensity $a_0 = 350$ ($I \sim 10^{23}$ W/cm^2), as illustrated in Fig. 1. The laser pulse has a duration of $\tau_p = 25$ fs, a wavelength of $\lambda_0 = 800$ nm, and a focal radius of $w_0 = 5\lambda_0$. The pulse energy is approximately 1 kJ, with a peak power of about 100 PW, achievable with next-generation laser facilities [39]. The simulated electron beam consists of 10^6 electrons with a transversely Gaussian distribution. The length of the electron beam is $L = 5\lambda_0$, with a radius of λ_0. The initial longitudinal position of the electron does not significantly affect its dynamics in the laser fields, as the Rayleigh length $z_R \gg L$. Without loss of generality, we assume a longitudinally uniform electron beam. The angular spread of the electron beam is $\Delta\theta = 2$ mrad, and the energy spread is $\Delta\varepsilon/\varepsilon = 5\%$, which are typical parameters for electron beams accelerated by laser wakefield acceleration and conventional accelerators.

The simulation results for the angular distribution of positron density are shown in Fig. 2. The VP causes a decrease of positron yield from $N_{\rm nvp} \approx 1.2 \times 10^7$ to $N_{\rm vp} \approx 1.17 \times 10^7$, implying a relative difference of $R = (N_{\rm nvp} - N_{\rm vp})/N_{\rm vp} \approx 1.8\%$ induced by neglecting VPE. In the quantum radiation-dominated regime (QRDR), where $R_c = \alpha a_0 \approx 1$, $\chi_e \gtrsim 1$ [6], most of the produced pairs experience significant radiation and are reflected in the direction of laser propagation (∼70%), while a small portion of positrons (∼30%) move forward into a small deflection angle; see Fig. 2(c). VP reshapes the angular distribution of positrons, leading to more passing through the laser and fewer being reflected compared to when it is absent; see Figs. 2(d) and 2(e). More intuitively, for small-angle positrons with $|\theta_x| \lesssim 100$ mrad and $|\theta_y| \lesssim 1$ mrad, the positron yield increases from $N_{\rm nvp} \approx 5.03 \times 10^4$ to $N_{\rm vp} \approx 5.76 \times 10^4$ in the case of VP; see Figs. 2(a) and 2(b). The relative difference induced by VP is $R \approx 12.64\%$, which is significantly higher compared to $R \approx 1.8\%$ for the entire beam and $R \approx 2.3\%$ for the reflected positrons; see Fig. 2(d).

Moreover, besides its impact on positron yield, VP also affects the positron spectrum, as shown in Fig. 3. VP results in the enhancement of positron yield in the high-energy regime ($\varepsilon_+ \gtrsim 129$ MeV). For the positrons with $\varepsilon_+ \gtrsim 1$ GeV, the average energy increases from $\bar{\varepsilon}_+^{\rm nvp} = 219$ MeV to $\bar{\varepsilon}_+^{\rm vp} = 237$ MeV, and the difference in pair yield increases to $R \sim 34.12\%$. The differences in angular distribution and spectrum indicate that incorporating VP is crucial for accurately describing the pair properties. More importantly, the VP alters scaling law of the pair yield with respect to both the deflection angle [Fig. 2(e)] and positron energy (Fig. 3), offering a potential method for measuring VP.

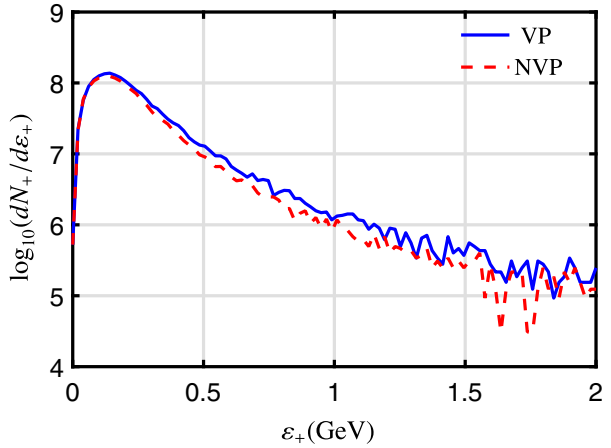

FIG. 3. The spectrum of positrons within $|\theta_x| \lesssim 100$ mrad and $|\theta_y| \lesssim 1$ mrad, with (blue solid line) and without VPE (red dashed line).

To analyze how VP influences the pair yield, we traced the trajectories of gamma photons that decay into pairs; see Fig. 4. The electrons emit substantial photons at the laser front, which are primarily composed of photons with energies in the hundreds of MeV; see Figs. 4(a) and 4(e). The average polarization of the emitted photons by unpolarized electrons (positrons) can be estimated using [20,35]

$$\xi_1 = \xi_2 = 0,$$
$$\xi_3 = \mathrm{K}_{\frac{2}{3}}(z_q)\left[\frac{\varepsilon^2+\varepsilon'^2}{\varepsilon'\varepsilon}\mathrm{K}_{\frac{2}{3}}(z_q) - \int_{z_q}^{\infty} dx \mathrm{K}_{\frac{1}{3}}(x)\right]^{-1}, \quad (3)$$

where $z_q = \frac{2}{3}\frac{\omega}{\chi_e \varepsilon'}$ with ε and ε' being the electron (positron) energy before and after emission, respectively. For the majority of the emission, where the photon energy satisfies $\omega \ll \varepsilon$, it follows that $\xi_1 = \xi_2 = 0$ and $\xi_3 \approx 0.5$, as indicated by Eq. (3) [Fig. 4(e)]. According to Eq. (1), vacuum birefringence has negligible effects on photons with $\xi_1 = \xi_2 = 0$. It is vacuum dichroism that plays a crucial role in altering the polarization of emitted photons as they travel through the laser. Vacuum dichroism induces a change in ξ_3 following [12,20]

$$\frac{d\xi_3}{dt} = \int \frac{\alpha m^2 d\varepsilon}{\sqrt{3}\pi\omega^2}(1-\xi_3^2)\mathrm{K}_{\frac{2}{3}}(z_p). \quad (4)$$

Photons initially generated with $\xi_3 \approx 0.5$ undergo an increased degree of polarization due to the influence of vacuum dichroism. Since the rate of variation is primarily governed by the photon energy through the $\mathrm{K}_{\frac{2}{3}}(z_p)$ term, higher-energy photons acquire larger ξ_3 traveling through the laser field [Fig. 4(e)].

Furthermore, the probability of pair production depends on photon polarization [40]:

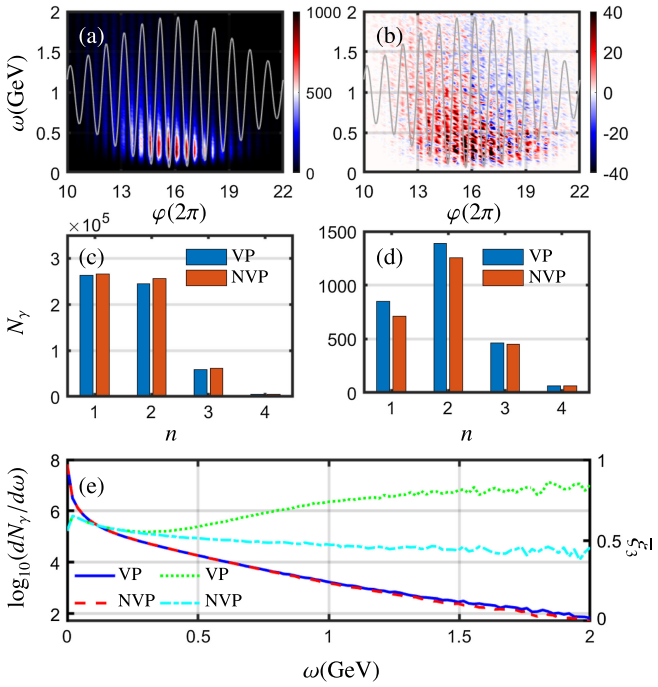

FIG. 4. The photon density $d^2N_\gamma/d\omega d\varphi$ with VPE (a) and the difference of pair yield $N_{\mathrm{nvp}} - N_{\mathrm{vp}}$ (b) versus pair production phase $\varphi(2\pi)$ and photon energy ω (GeV). The superimposed gray lines in (a) and (b) represent the x component of the electric fields. (c) The total photon number N_γ that decays into pairs versus photon generations n. (d) The same as (c) but for the photons that produce pairs within $|\theta_x| \lesssim 100$ mrad and $|\theta_y| \lesssim 1$ mrad. (e) Photon spectra with (solid blue line) and without (red dashed line) VPE. The average photon polarization ξ_3 versus photon energy ω (GeV) with (green dotted line) and without (cyan dot-dashed line) VPE.

$$dW^P = \frac{\alpha m^2 d\varepsilon}{\sqrt{3}\pi\omega^2}\left\{\int_{z_p}^{\infty} dx \mathrm{K}_{\frac{1}{3}}(x) + \frac{\varepsilon_+^2+\varepsilon^2}{\varepsilon\varepsilon_+}\mathrm{K}_{\frac{2}{3}}(z_p) - \xi_3 \mathrm{K}_{\frac{2}{3}}(z_p)\right\}. \quad (5)$$

Consequently, high-energy photons can penetrate deeper into the laser to produce pairs at the tail, due to the enhancement of ξ_3. As shown in Fig. 4(b), incorporating VPE induces a phase delay in pair production, reducing the positron yield at the laser front while enhancing it at the laser tail. The positrons generated in the front are likely to be reflect due to the dramatic radiation reaction near laser peak. In contrast, these generated in the pulse tail have higher energy and experience less radiation reaction. As a result, they tend to move forward with a small deflection angle. Consequently, both the positron yield and energy within $|\theta_x| \lesssim 100$ mrad and $|\theta_y| \lesssim 1$ mrad increase when VPE is considered; see Figs. 2 and 3. The phase delay induced by vacuum dichroism is evident in the reflection geometry. Without it, pairs produced at different phases

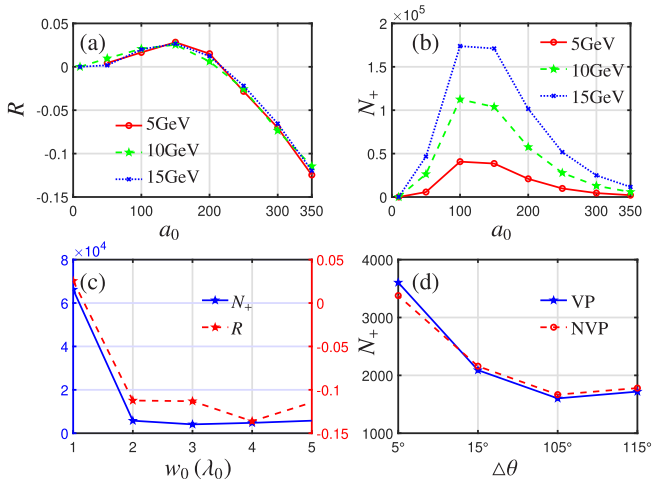

FIG. 5. The scaling law of R (a) and pair number N_+ (b) versus a_0 for electrons with initial energy of 5 (red solid line), 10 (green dashed line), and 15 GeV (blue dotted line). (c) The scaling law of R (red solid line) and pair number N_+ (blue dashed line) versus laser spot size w_0 for $\varepsilon_0 = 10$ GeV, $a_0 = 350$, $|\theta_x| \lesssim 100$ mrad, and $|\theta_y| \lesssim 1$ mrad. (d) The scaling law of N_+ within $\delta\theta = 10°$ and $\phi \in (-1°, 1°)$ versus deflection angle $\Delta\theta = \pi - \theta$ for $w_0 = 2\lambda_0$ with (blue solid line) and without (red dashed line) VPE. The initial electron number $N_e = 10^5$.

would mix within a small deflection angle, diminishing the strength of the VP signal.

Meanwhile, even though multiple emissions occur in the QRDR, the difference in pair yield is primarily driven by the first and secondary photon emissions; see Figs. 4(c) and 4(d). Compared with the third and fourth generations, the first two generations are more energetic and are produced in an earlier phase, resulting in a larger ξ_3 and, consequently, a more pronounced difference in pair yield.

We further studied the impacts of the laser and electron beam parameters on the relative difference R, as shown in Fig. 5(a). The relative difference in pair yield depends on the laser intensity, while there is no particularly strong correlation with respect to the energy of the initial electrons. For $a_0 \lesssim 100$, we have $0 < R < 3\%$, indicating that the pair yield is larger when VP is ignored and that the relative difference is rather small. This is because the particles in a relatively week field tend to move forward rather than being reflected. Without reflection geometry, the copious pairs produced at the laser front, where $R > 0$, are mixed with those from the laser tail, where $R < 0$, and result in a small positive R. As the laser intensity increases to $100 < a_0 < 200$, we enter a relatively stable region where $R \approx 3\%$ and the pair yield reaches its peak at $N \approx 1.7 \times 10^5$, implying that VP measurement may be feasible with current laser technology. As a_0 further increases to the QRDR, pairs produced at the laser front lose substantial energy and are reflected, isolating the pairs generated by energetic photons at the laser tail. These pairs exhibit a stronger negative R. It is important to note that, although R is significantly enhanced in an extremely intense laser field, the pair yield at small angles decreases [Fig. 5(b)]. This results in larger statistical errors and poses challenges for experimental measurement.

The impact of laser spot size is illustrated in Figs. 5(c) and 5(d). For a tightly focused laser beam with $w_0 = 1\lambda_0$, most pairs experience a weakened field and move forward, significantly enhancing the pair yield at small angles. However, the relative difference $R = 2.55\%$ is rather small in the forward scattering case. As the laser spot size increases to $w_0 \geq 2\lambda_0$, the interaction enters the reflection regime, where both N_+ and R decrease sharply and then stabilize around $N_+ \sim 10^3$ and $R \sim -10\%$, respectively. This trend indicates that the observable R is robust over a wide range of spot size, i.e., $w_0 \in [2\lambda_0, 5\lambda_0]$. However, in a laser field with a large spot size, VP induces significant modifications to the angular distribution [Fig. 2(e)], which are not observed for smaller spot sizes [Fig. 5(d)]. For $w_0 = 5\lambda_0$, strong reflection causes N_+ to increase with the deflection angle $\Delta\theta$. The presence of VP enhances N_+ at small $\Delta\theta$, disrupting the otherwise monotonic increase of N_+ with $\Delta\theta$. In contrast, for a smaller laser spot size of $w_0 = 2\lambda_0$, fewer pairs are reflected compared to the $w_0 = 5\lambda_0$ case, resulting in a decrease of N_+ with increasing $\Delta\theta$. In this scenario, the VP-induced enhancement at small $\Delta\theta$ does not alter the overall scaling behavior of N_+ with $\Delta\theta$, as the pair number decreases with deflection angle regardless of VP. Therefore, the VP signal in the small-angle region ($|\theta_x| \lesssim 100$ mrad and $|\theta_y| \lesssim 1$ mrad) remains robust against variations in laser spot size. However, a larger beam size is preferred to reveal additional VP signatures in the angular distribution.

Furthermore, we conducted a simulation with the collision angle $\theta_c = 17.2°$, as employed in the Laser Und XFEL experiment (LUXE). The simulation results for the angular distribution of positron density are shown in Fig. 6. Although the total pair yield decreases slightly from $N_{\rm vp} \approx 1.17 \times 10^7$ to $N_{\rm vp} \approx 9.0 \times 10^6$ as the collision angle increases from $\theta_c = 0°$ to $\theta_c = 17.2°$, the relative difference R induced by vacuum polarization is barely changed. Specifically, for the oblique collision at $\theta_c = 17.2°$, the VP causes a decrease of positron yield from $N_{\rm nvp} \approx 9.17 \times 10^6$ to $N_{\rm vp} \approx 9.0 \times 10^6$, implying a relative difference of $R = (N_{\rm nvp} - N_{\rm vp})/N_{\rm vp} \approx 1.92\%$ induced by neglecting VPE. This observable $R = 1.92\%$ at $\theta_c = 17.2°$ is roughly the same with $R = 1.8\%$ for $\theta_c = 0°$. Moreover, in head-on collisions, the pairs are concentrated at $\theta_y = 0$, whereas they shift toward $\theta_y = 300$ mrad in oblique collisions; see Figs. 6(a)–6(c). However, in both cases, VP reshapes the angular distribution of positrons, leading to more passing through the laser and fewer being reflected compared to when it is absent; see Figs. 6(d) and 6(e). More intuitively, for small-angle positrons with $|\theta_x| \lesssim 100$ mrad and $300 \lesssim \theta_y \lesssim 302$ mrad, the positron yield increases from $N_{\rm nvp} \approx 2.12 \times 10^4$ to

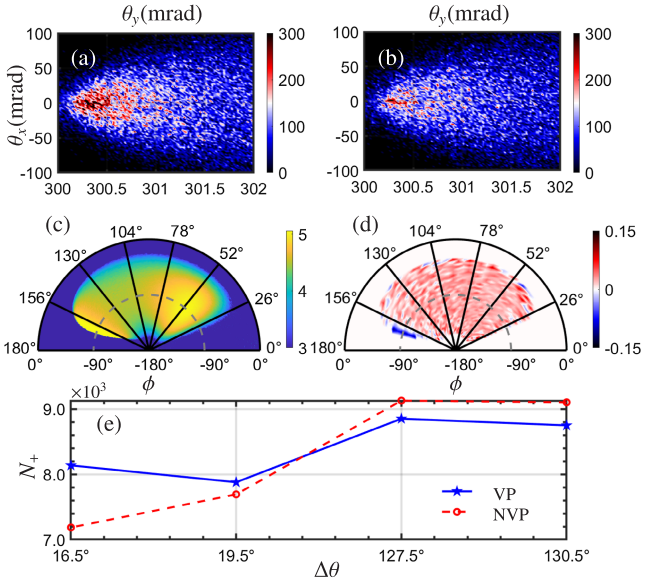

FIG. 6. The angular distribution of positron density $d^2N_+/d\theta_x d\theta_y$ within $|\theta_x| \lesssim 100$ mrad and $300 \lesssim \theta_y \lesssim 302$ mrad versus $\theta_x = \tan^{-1} p_x/p_z$ (mrad) and $\theta_y = \tan^{-1} p_y/p_z$ (mrad) for the cases with (a) and without (b) VPE. Angular distribution of positrons density $\log_{10}(dN_+/d\Omega)$ (c) and density difference R (d) versus the polar angle θ (degree, black solid scale) and azimuthal angle ϕ (degree, gray dashed scale). (e) The scaling law of positron yield N_+ within $\delta\theta = 3°$ and $\phi \in (-91°, -89°)$ versus deflection angle $\Delta\theta = \pi - \theta$ for the cases with (blue solid line) and without (red dashed line) VPE. The collision angle between the laser pulse and the initial electron beam is $\theta_c = \tan^{-1} p_y/p_z = 17.2°$.

$N_{\rm vp} \approx 2.57 \times 10^4$ in the case of VP; see Figs. 6(a) and 6(b). The relative difference induced by VP is $R \approx 17.3\%$, which is roughly consistent with $R \approx 12.64\%$ in the head-on collision scenario. Therefore, our scheme is robust against variation in collision angle. To ensure optimal temporal and spatial alignment during the interaction, the laser jitter should be kept smaller than the Rayleigh length. In a recent collision experiment, the temporal jitter was approximately 11 fs [41], which is significantly smaller than the Rayleigh length $z_R = \pi w_0^2/\lambda_0 = 210$ fs for $w_0 = 5\lambda_0$.

Considering a realistic electron beam charge of a few nC, the total charge of detected positrons would be around tens of pC. So, to detect VP signal, one would need to measure positron charge at different angles with an accuracy sufficiently better than 1 pC. Precise diagnostics of sub-pC-level particle bunches can be achieved with techniques such as turbo-ICT (integrating current transformer) [42], scintillating screens [43–45], imaging plates [46], and DRZ-high screens [47]. Furthermore, the LUXE silicon pixel tracking detector has been designed for the precise measurement of the rate and energy of the nonlinear Breit-Wheeler e^+e^- pairs [43], which allows the unambiguous measurement of the pair yield ranging from $\sim\mathcal{O}(10^{-3})$ to $\sim\mathcal{O}(10^6)$. The tracker is based on the technology developed for the upgrade of the inner tracking system of the ALICE experiment at the LHC and particularly the state-of-the-art "ALice PIxel DEtector" monolithic active pixel sensors at its heart. Therefore, it is feasible to measure the positron's angular distribution with current detectors.

In conclusion, we explored VPE through nonlinear Compton scattering of an unpolarized electron beam with a linearly polarized strong laser. Unlike the traditional two-stage approach, which requires the preparation of a highly polarized and well-collimated photon beam, our method simplifies the process by utilizing a single collision with an unpolarized electron beam. During the collision, the vacuum dichroism induces an increase in ξ_3 for the emitted gamma photons, resulting in a decrease in the overall pair yield (∼1.8%) and causing a phase delay in the pair production for high-energy photons. In a reflection scenario, this phase delay further alters the angular distribution of the produced pairs, particularly in the small-angle regions, with $|\theta_x| \lesssim 100$ mrad and $|\theta_y| \lesssim 1$ mrad. In this angle region, vacuum dichroism enhances both the yield and energy of the produced pairs. The relative difference from neglecting VPE can reach up to 40%, highlighting the importance of including VPE in high-field QED simulations. Additionally, measuring the energy spectrum and angular distribution of pairs provides information about the intermediate photon polarization, revealing the effects of vacuum polarization without the challenges associated with polarization measurements. Thus, our approach, which relies on pair yield as a signal, may provide a more feasible method for measuring VP.

We gratefully acknowledge helpful discussions with Karen Z. Hatsagortsyan. This work is supported by the National Key R&D Program of China (Grant No. 2021YFA1601700) and the National Natural Science Foundation of China (Grants No. 12474312 and No. 12074262).

[1] G. Zavattini, U. Gastaldi, R. Pengo, G. Ruoso, F. D. Valle, and E. Milotti, Measuring the magnetic birefringence of vacuum: The PVLAS experiment, Int. J. Mod. Phys. A **27**, 1260017 (2012).

[2] A. Ejlli, F. Della Valle, U. Gastaldi, G. Messineo, R. Pengo, G. Ruoso, and G. Zavattini, The PVLAS experiment: A 25 year effort to measure vacuum magnetic birefringence, Phys. Rep. **871**, 1 (2020).

[3] A. Cadène, P. Berceau, M. Fouché, R. Battesti, and C. Rizzo, Vacuum magnetic linear birefringence using pulsed fields: Status of the BMV experiment, Eur. Phys. J. D **68**, 1 (2014).

[4] E. Zavattini, G. Zavattini, G. Ruoso, E. Polacco, E. Milotti, M. Karuza, U. Gastaldi, G. Di Domenico, F. Della Valle, R. Cimino *et al.*, Experimental observation of optical rotation generated in vacuum by a magnetic field, Phys. Rev. Lett. **96**, 110406 (2006).

[5] M. Marklund and P. K. Shukla, Nonlinear collective effects in photon-photon and photon-plasma interactions, Rev. Mod. Phys. **78**, 591 (2006).

[6] A. Di Piazza, C. Müller, K. Hatsagortsyan, and C. H. Keitel, Extremely high-intensity laser interactions with fundamental quantum systems, Rev. Mod. Phys. **84**, 1177 (2012).

[7] H.-P. Schlenvoigt, T. Heinzl, U. Schramm, T. E. Cowan, and R. Sauerbrey, Detecting vacuum birefringence with x-ray free electron lasers and high-power optical lasers: A feasibility study, Phys. Scr. **91**, 023010 (2016).

[8] B. Shen, Z. Bu, J. Xu, T. Xu, L. Ji, R. Li, and Z. Xu, Exploring vacuum birefringence based on a 100 PW laser and an x-ray free electron laser beam, Plasma Phys. Controlled Fusion **60**, 044002 (2018).

[9] D. Xu, B. Shen, J. Xu, and Z. Liang, XFEL beamline design for vacuum birefringence experiment, Nucl. Instrum. Methods Phys. Res., Sect. A **982**, 164553 (2020).

[10] Y. Nakamiya and K. Homma, Probing vacuum birefringence under a high-intensity laser field with gamma-ray polarimetry at the GeV scale, Phys. Rev. D **96**, 053002 (2017).

[11] B. King and N. Elkina, Vacuum birefringence in high-energy laser-electron collisions, Phys. Rev. A **94**, 062102 (2016).

[12] S. Bragin, S. Meuren, C. H. Keitel, and A. Di Piazza, High-energy vacuum birefringence and dichroism in an ultrastrong laser field, Phys. Rev. Lett. **119**, 250403 (2017).

[13] A. Macleod, J. Edwards, T. Heinzl, B. King, and S. Bulanov, Strong-field vacuum polarisation with high energy lasers, New J. Phys. **25**, 093002 (2023).

[14] V. N. Baier, V. M. Katkov, and V. M. Strakhovenko, *Electromagnetic Processes at High Energies in Oriented Single Crystals* (World Scientific, Singapore, 1998).

[15] V. N. Baier, A. Milshtein, and V. Strakhovenko, Interaction between a photon and an intense electromagnetic wave, Sov. Phys. JETP **42**, 961 (1975), http://www.jetp.ras.ru/cgi-bin/e/index/e/42/6/p961?a=list.

[16] W. Becker and H. Mitter, Vacuum polarization in laser fields, J. Phys. A **8**, 1638 (1975).

[17] S. Meuren, C. H. Keitel, and A. Di Piazza, Polarization operator for plane-wave background fields, Phys. Rev. D **88**, 013007 (2013).

[18] G. Torgrimsson, Loops and polarization in strong-field QED, New J. Phys. **23**, 065001 (2021).

[19] B. King, T. Heinzl, and T. Blackburn, Strong field vacuum birefringence in plane wave pulses, Eur. Phys. J. C **83**, 901 (2023).

[20] Y.-N. Dai, K. Z. Hatsagortsyan, C. H. Keitel, and Y.-Y. Chen, Fermionic signal of vacuum polarization in strong laser fields, Phys. Rev. D **110**, 012008 (2024).

[21] D. C. Hutchings, M. Sheik-Bahae, D. J. Hagan, and E. W. Van Stryland, Kramers-Krönig relations in nonlinear optics, Opt. Quantum Electron. **24**, 1 (1992).

[22] J. S. Toll, *The Dispersion Relation for Light and Its Application to Problems Involving Electron Pairs* (Princeton University, Princeton, NJ, 1952).

[23] J. Adam, L. Adamczyk, J. Adams, J. Adkins, G. Agakishiev, M. Aggarwal, Z. Ahammed, I. Alekseev, D. Anderson, A. Aparin *et al.*, Measurement of e^+e^- momentum and angular distributions from linearly polarized photon collisions, Phys. Rev. Lett. **127**, 052302 (2021).

[24] O. Borysov, B. Heinemann, A. Ilderton, B. King, and A. Potylitsyn, Using the nonlinear Breit-Wheeler process to test nonlinear vacuum birefringence, Phys. Rev. D **106**, 116015 (2022).

[25] A. Apyan, R. Avakian, B. Badelek, S. Ballestrero, C. Biino, I. Birol, P. Cenci, S. Connell, S. Eichblatt, T. Fonseca *et al.*, Coherent bremsstrahlung, coherent pair production, birefringence, and polarimetry in the 20–170 GeV energy range using aligned crystals, Phys. Rev. Accel. Beams **11**, 041001 (2008).

[26] H. Abramowicz, U. Acosta, M. Altarelli, R. Assmann, Z. Bai, T. Behnke, Y. Benhammou, T. Blackburn, S. Boogert, O. Borysov *et al.*, Conceptual design report for the LUXE experiment, Eur. Phys. J. Special Topics **230**, 2445 (2021).

[27] A. Narayan, D. Jones, J. Cornejo, M. Dalton, W. Deconinck, D. Dutta, D. Gaskell, J. Martin, K. Paschke, V. Tvaskis *et al.*, Precision electron-beam polarimetry at 1 GeV using diamond microstrip detectors, Phys. Rev. X **6**, 011013 (2016).

[28] K. Ozaki, S. Takahashi, S. Aoki, K. Kamada, T. Kaneyama, R. Nakagawa, and H. Rokujo, Demonstration of polarization sensitivity of emulsion-based pair conversion telescope for cosmic gamma-ray polarimetry, Nucl. Instrum. Methods Phys. Res., Sect. A **833**, 165 (2016).

[29] N. Elkina, A. Fedotov, I. Y. Kostyukov, M. Legkov, N. Narozhny, E. Nerush, and H. Ruhl, QED cascades induced by circularly polarized laser fields, Phys. Rev. Accel. Beams **14**, 054401 (2011).

[30] C. P. Ridgers, J. G. Kirk, R. Duclous, T. G. Blackburn, C. S. Brady, K. Bennett, T. D. Arber, and A. R. Bell, Modelling gamma-ray photon emission and pair production in high-intensity laser–matter interactions, J. Comput. Phys. **260**, 273 (2014).

[31] D. Green and C. Harvey, SIMLA: Simulating particle dynamics in intense laser and other electromagnetic fields via classical and quantum electrodynamics, Comput. Phys. Commun. **192**, 313 (2015).

[32] A. Gonoskov, S. Bastrakov, E. Efimenko, A. Ilderton, M. Marklund, I. Meyerov, A. Muraviev, A. Sergeev, I. Surmin, and E. Wallin, Extended particle-in-cell schemes for physics

in ultrastrong laser fields: Review and developments, Phys. Rev. E **92**, 023305 (2015).
[33] Y.-Y. Chen, P.-L. He, R. Shaisultanov, K. Z. Hatsagortsyan, and C. H. Keitel, Polarized positron beams via intense two-color laser pulses, Phys. Rev. Lett. **123**, 174801 (2019).
[34] Y.-F. Li, Y.-Y. Chen, W.-M. Wang, and H.-S. Hu, Production of highly polarized positron beams via helicity transfer from polarized electrons in a strong laser field, Phys. Rev. Lett. **125**, 044802 (2020).
[35] Y.-N. Dai, B.-F. Shen, J.-X. Li, R. Shaisultanov, K. Z. Hatsagortsyan, C. H. Keitel, and Y.-Y. Chen, Photon polarization effects in polarized electron–positron pair production in a strong laser field, Matter Radiat. Extremes **7**, 014401 (2022).
[36] K.-H. Zhuang, Y.-Y. Chen, Y.-F. Li, K. Z. Hatsagortsyan, and C. H. Keitel, Laser-driven lepton polarization in the quantum radiation-dominated reflection regime, Phys. Rev. D **108**, 033001 (2023).
[37] Y.-F. Li, Y.-Y. Chen, K. Z. Hatsagortsyan, A. Di Piazza, M. Tamburini, and C. Keitel, Strong signature of one-loop self-energy in polarization resolved nonlinear Compton scattering, Phys. Rev. D **107**, 116020 (2023).
[38] Y.-F. Li, Y.-Y. Chen, K. Z. Hatsagortsyan, and C. H. Keitel, Helicity transfer in strong laser fields via the electron anomalous magnetic moment, Phys. Rev. Lett. **128**, 174801 (2022).
[39] C. N. Danson, C. Haefner, J. Bromage, T. Butcher, J.-C. F. Chanteloup, E. A. Chowdhury, A. Galvanauskas, L. A. Gizzi, J. Hein, D. I. Hillier *et al.*, Petawatt and exawatt class lasers worldwide, High Power Laser Sci. Eng. **7**, e54 (2019).
[40] Y.-Y. Chen, K. Z. Hatsagortsyan, C. H. Keitel, and R. Shaisultanov, Electron spin-and photon polarization-resolved probabilities of strong-field QED processes, Phys. Rev. D **105**, 116013 (2022).
[41] M. Mirzaie, C. I. Hojbota, D. Y. Kim, V. B. Pathak, T. G. Pak, C. M. Kim, H. W. Lee, J. W. Yoon, S. K. Lee, Y. J. Rhee *et al.*, All-optical nonlinear Compton scattering performed with a multi-petawatt laser, Nat. Photonics **18**, 1212 (2024).
[42] K. Nakamura, D. Mittelberger, A. Gonsalves, J. Daniels, H. Mao, F. Stulle, J. Bergoz, and W. Leemans, Pico-coulomb charge measured at BELLA to percent-level precision using a Turbo-ICT, Plasma Phys. Controlled Fusion **58**, 034010 (2016).
[43] H. Abramowicz, M. Almanza Soto, M. Altarelli, R. Aßmann, A. Athanassiadis, G. Avoni, T. Behnke, M. Benettoni, Y. Benhammou *et al.* (L. Collaboration), Technical design report for the LUXE experiment, Eur. Phys. J. Special Topics **233**, 1709 (2024).
[44] K. Poder, M. Tamburini, G. Sarri, A. Di Piazza, S. Kuschel, C. Baird, K. Behm, S. Bohlen, J. Cole, D. Corvan *et al.*, Experimental signatures of the quantum nature of radiation reaction in the field of an ultraintense laser, Phys. Rev. X **8**, 031004 (2018).
[45] J. Cole, K. Behm, E. Gerstmayr, T. Blackburn, J. Wood, C. Baird, M. J. Duff, C. Harvey, A. Ilderton, A. Joglekar *et al.*, Experimental evidence of radiation reaction in the collision of a high-intensity laser pulse with a laser-wakefield accelerated electron beam, Phys. Rev. X **8**, 011020 (2018).
[46] N. Nakanii, K. Kondo, T. Yabuuchi, K. Tsuji, K. Tanaka, S. Suzuki, T. Asaka, K. Yanagida, H. Hanaki, T. Kobayashi *et al.*, Absolute calibration of imaging plate for GeV electrons, Rev. Sci. Instrum. **79**, 066102 (2008).
[47] Y. Wu, J. Hua, Z. Zhou, J. Zhang, S. Liu, B. Peng, Y. Fang, X. Ning, Z. Nie, F. Li *et al.*, High-throughput injection–acceleration of electron bunches from a linear accelerator to a laser wakefield accelerator, Nat. Phys. **17**, 801 (2021).